Conference Proceedings
International Conference on Mechanical and Aerospace Engineering (ICAMAE 2023)
28th to 30th November 2023

The application of symmetrical motorised momentum exchange tethers for two-way Earth-Mars transportation

Shem S. Afonso, Matthew P. Cartmell
Department of Mechanical and Aerospace Engineering, University of Strathclyde
68 Montrose Street, Glasgow, G1 1RS, Scotland, United Kingdom
shem.afonso.2022@uni.strath.ac.uk ; matthew.cartmell@strath.ac.uk

ABSTRACT

This paper presents a novel strategy for the use of symmetrical motorised momentum exchange tethers for a two-way continuous payload transfer system between Earth and Mars. Symmetrical tethers do not necessarily deorbit on payload capture and release because there is no change in the geometrical location of the centre of mass when in operation. A novel strategy is proposed requiring two tethers, whereby one rotates prograde and the other retrograde, and two dummy payloads in suitable parking orbits around each planet to provide overall mass balance. Two additional outrigger payloads are tethered to the stator side of the central drive motor facility to provide a counter inertia against which the primary propulsion side rotates. If the two sides of the motor facility are reasonably balanced, they will contra-rotate effectively, facilitating spin-up of the tether and reset to desired initial conditions for subsequent phases. A methodology has been developed to calculate the orbits of the tethers and the dummy payloads around Earth and Mars, and a drag perturbation analysis has been carried out on selected sets of results to determine the orbit decay. Finally, some major failure scenarios are discussed and some recovery options are proposed.

Keyword: - *Motorised tethers, symmetry, momentum exchange, two-way interplanetary propulsion.*

NOMENCLATURE

a_i	=	Semi major axis of i^{th} orbit	r_{Pi}	=	Radius of point P on i^{th} orbit
COM	=	Centre of mass	S	=	Frontal area of payload / tether motor facility
C_D	=	Coefficient of drag of dummy payload or tether	SOI	=	Sphere of Influence
			T1	=	Tether 1
d1	=	Dummy payload 1	T2	=	Tether 2
d2	=	Dummy payload 2	t	=	Time
HET	=	Hyperbolic escape trajectory	u	=	Displacement in required direction
HRT	=	Hyperbolic return trajectory	$\bar{u}$	=	Displacement vector
L_1	=	Sub-span of tether 1	V_∞	=	Excess velocity – the velocity the payload has with respect to the sun when it just exits or enters the planet's sphere of influence
L_2	=	Sub-span of tether 2			
l	=	Orbital harmonic - relates time period of orbit 2 to orbit 1			
MMET	=	Motorised momentum exchange tether	V_{Pi}	=	Velocity at point P on i^{th} orbit
m	=	Orbital harmonic. Relates time period of orbit 3 to orbit 2	V_x	=	Velocity in x direction
			V_y	=	Velocity in y direction
m_p	=	Mass of tether motor facility or dummy payload	x	=	Displacement in x direction
			y	=	Displacement in y direction
n	=	Orbital harmonic - relates time period of orbit 5 to orbit 3	μ_E	=	Gravitational parameter of Earth
			μ_M	=	Gravitational parameter of Mars
P_i	=	Time period of i^{th} orbit	μ_S	=	Gravitational parameter of Sun
p1	=	Payload 1	ω_{t1}	=	In-plane tether 1 angular velocity
p2	=	Payload 2	ω_{t2}	=	In-plane tether 2 angular velocity
R_E	=	Radius of Earth			
R_M	=	Radius of Mars			
r_E	=	Radius of Earth's orbit around Sun			
r_M	=	Radius of Mars' orbit around Sun			

1 INTRODUCTION

A space tether is a long line that orbits a planet, and if left unperturbed, will usually orient vertically i.e., along the gravity vector. This orientation is also a stable position due to the gravity gradient effect. The orbit of the tether passes through the centre of mass (COM) of the tether. The entire space tether in vertical orientation orbits around the planet with the same angular velocity as its COM. This causes the upper end of the tether which is further away from the planet to travel at a higher velocity than the lower end. We know that as we go further away from a planet, the velocity required to orbit the planet decreases until it theoretically becomes zero at infinity. But the upper end of the tether has a higher velocity than would be required by a satellite or payload orbiting at the same altitude. Similarly, the lower end of the tether has a lower velocity than would be required by a satellite or payload orbiting at that altitude. If we consider a symmetrical tether, as discussed in this paper, in vertical orientation and carrying payloads of equal mass at each end while it is orbiting the planet in a circular orbit as shown in Figure 1 (left), then the attached payloads will also orbit the planet in a circular trajectory. When both payloads are detached from the tether, the upper payload will go in a higher elliptical orbit and the lower payload will go in a lower elliptical orbit. This is shown in Figure 1 (right). The point of release of the upper payload will become the periapsis of its orbit and that of the lower payload will be the apoapsis of its orbit. Therefore, tethers can be used for imparting delta-v (change in velocity) without the use of any propellant. Additionally, tethers can generate extra delta-v by catching a payload at the lower end, transferring it to the higher end and releasing it, or vice versa, and also through monotonic rotation. If that rotation is generated by a motor facility then the tethers are termed Motorised Momentum Exchange Tethers (MMETs).

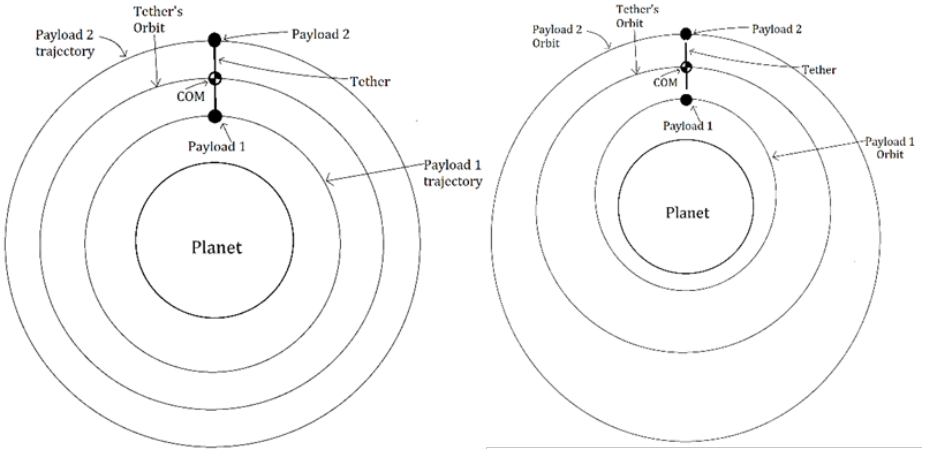

Figure 1: An example of a symmetrical tether imparting delta-v to payloads. (left) before release, (right) after release

Several studies have been conducted on the use of space tethers for lunar and interplanetary travel. Puig-Suari *et al.* [1] analysed uniform and tapered tethers for interplanetary missions. A tapered tether has the advantage of bearing higher centrifugal loads and thus can achieve higher tip speeds compared to a uniform tether. Forward and Nordley [2] proposed a 'Mars-Earth Rapid Interplanetary Tether Transport' (MERITT) system that has an asymmetrical rotating tether orbiting Earth and Mars in a highly elliptical orbit. The system is capable of generating a tether tip velocity of around 2.5 km/s which will enable travel between Earth and Mars in around 90 days. The authors proposed extending the system to other planets and moons thus creating a tether transportation system within the solar system. Cartmell and Ziegler [3] proposed an architecture for continuous Earth-Moon payload exchange using symmetrically laden tethers. The paper proposes a three tethers system where two tethers orbit the Earth and one tether, defined as a *Lunavator* orbits the Moon. Hoyt and Uphoff [4] designed an architecture for repeated transfer of payload between Earth and Moon using two asymmetrical tethers with electrodynamic re-boost. Accettura *et al.* [5] assessed the viability of a mission to Mars using a combination of different propulsion methods. They assessed the effectiveness of coupling a nuclear engine with a pulsed plasma thruster along with tethered systems for generating artificial gravity. Jokic and Longuski [6] studied the design of an asymmetrical tether placed on Phobos to enable a transfer to Earth from Mars. The study examined different mission scenarios, shapes of tethers, and material composition. The authors recommended the use of tapered tethers to maximise the efficiency and strength of the tether. Knapman and Swan [7] proposed the use of tethers on a 100,000 km long space elevator. The facility designed is capable of generating velocities as high as 17 km/s which reduces the travel time to Mars to nearly 60 days. Previous research has explored the use of tethers to facilitate payload transfer between Earth and Mars. However, these studies primarily focused on asymmetrical tethers.

The aim of this study is to address this existing gap by developing a conceptual symmetrical MMET logistic system for continuous two-way transfer of payloads between Earth and Mars. The use of symmetrical tethers has been proposed because they offer the advantage of maintaining their orbit during the simultaneous capture or release of equal payloads at both their ends, thus eliminating the need to readjust their orbit. The approach followed by Cartmell and Ziegler [3] to design a conceptual tether system for two-way continuous transfers between Earth and Moon has been used as a basis for strategy development. However, if that exact strategy is followed then there are certain limitations imposed by the transfer time between the two planets and the wait time until the next transfer window, as explained in the following section. Hence, the use of dummy payloads has been proposed whose sole purpose is to balance the tethers and eliminate the above-mentioned limitations. This paper presents a novel strategy for tether layout around Earth and Mars with the use of dummy payloads, methodology to find the parameters of the orbits of the tethers, payloads and dummy payloads, major failure scenarios that can occur and a possible recovery strategy and drag perturbation study. Since this is a preliminary study, it is assumed that the orbits of Earth and Mars around the Sun are circular and coplanar. Additionally, the planets are assumed to be spherical, hence negating any J2 perturbation.

The orbital parameters of Earth's and Mars's orbit, gravitational parameters and radius of Earth and Mars are shown in Table 1.

Table 1: Orbital parameters of Earth's and Mars's orbit around the Sun and gravitational parameters

Parameter	Description	Value
μ_S	Gravitational Parameter of Sun	$1.327*10^{11}$ km^3/s^2
μ_E	Gravitational Parameter of Earth	$3.986*10^5$ km^3/s^2
μ_M	Gravitational Parameter of Mars	$4.283*10^4$ km^3/s^2
r_E	Radius of Earth's orbit around Sun	$1.496*10^8$ km
r_M	Radius of Mars's orbit around Sun	$2.279*10^8$ km
R_E	Radius of Earth	6378 km
R_M	Radius of Mars	3389.9 km

2 LIMITATION IMPOSED BY TRANSFER TIME AND WAIT TIME

The transfer type between Earth and Mars and vice versa considered in this study is the Hohmann Transfer. The time of transfer and the wait time are calculated according to the procedure mentioned in Curtis [8]. The results are summarised in Table 2.

Table 2: Transfer time and wait time for Hohmann transfer between Earth and Mars

Type	Time
Transfer time (Hohmann) between Earth and Mars	$2.237*10^7$ s / 258.882 days
Wait time until the next transfer window for travel from Mars to Earth after the payload's arrival on Mars	$3.924*10^7$ s / 454.318 days
Wait time until the next transfer window for travel from Earth to Mars after the payload's arrival on Earth	$1.660*10^7$ s / 192.152 days

Extending the strategy of Cartmell and Ziegler [3] to this scenario, it is found that the payloads spend a long time, more than a year, in space attached to tethers. This happens due to the long wait time until the next transfer window and the dependency of the symmetrical tethers on payloads that arrive from the other planet in order to maintain symmetry. To eliminate this long wait time, unsymmetrical tethers (with Electrodynamic re-boost) [9] or dummy payloads whose purpose is to maintain the symmetry of tethers can be used. The focus of this study is to develop a strategy using dummy payloads.

3 TRANSFER PROCESS WITH THE USE OF DUMMY PAYLOADS

The conditions for the use of dummy payloads are:

- The MMET must not cause the dummy payload to escape the planet's sphere of influence (SOI).
- The MMET should not deorbit the dummy payload.
- Dummy payload orbits must be designed such that they can be reused again

The proposed strategy involves two tethers orbiting each planet. The tether that is closer to the planet, shown here as T1, rotates prograde and the other tether that is further away, shown here as T2, rotates retrograde. Figure 2 presents the four steps involved in the outgoing phase - transferring the payload from parking orbit 1 to Hyperbolic Escape Trajectory (HET) 4. The HET 4 is designed such that it has the required excess velocity to reach the other planet.

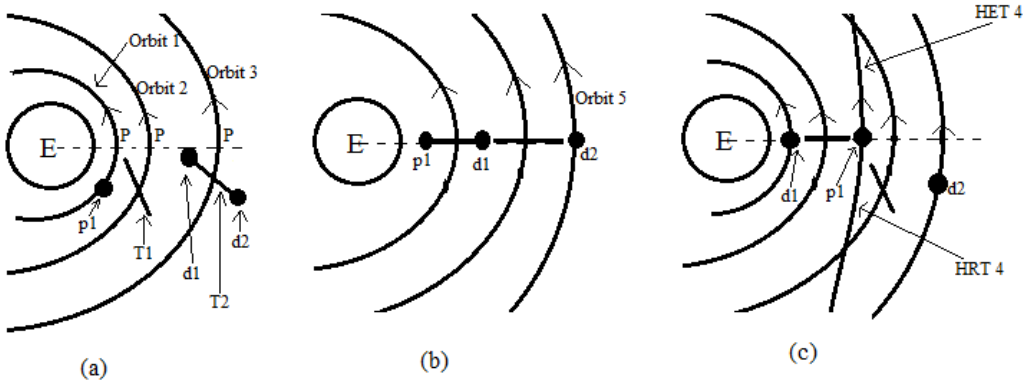

Figure 2: Outgoing phase (a) step 1, (b) step 2, (c) step 3

As seen from Figure 2, step 1 involves the desired payload, p1, which is to be sent to the other planet, already parked in orbit 1, and the two other dummy payloads, d1 and d2, attached to T2. In step 2, T1 captures p1 from orbit 1 and d1 from T2. T2 releases d2 in the dummy payload's parking orbit 5. In step 3, T1 releases p1 into HET 4 and d1 into orbit 1. The outgoing phase is complete after step 3.

During the return phase, the desired payload to be captured, say p1, arrives along a Hyperbolic Return Trajectory (HRT) 4. T1 captures p1 from HRT 4 and d1 from orbit 1, and so the above-described procedure happens in reverse order until payload p1 is released in parking orbit 1 and both dummy payloads are captured by T2. Payload p1 must de-orbit on its own using its own propulsion.

4 METHODOLOGY TO DETERMINE THE ORBITAL PARAMETERS, TETHER SUB-SPAN AND ANGULAR SPEED, BASED ON THE PROPOSED STRATEGY

There are two conditions to be met while designing the orbits of the tethers and the dummy payloads:

- The relative velocities during handovers/captures must be zero.
- The time period of the higher orbits must be some integral multiple of the time period of the lower orbits. This ensures that after a fixed interval of time, the tethers and payloads are in a straight line in order to enable capture/handover.

Point P marked on the orbits in Figure 2 (a) can be either the periapsis or the apoapsis. The opposite point is named Q, which is not shown in the Figures. Figure 3 shows the important distances and tether sub-span considered in this study. Note that E in the Figure represents planet Earth but can be Mars too. The sub-spans is the distance from the COM of the tether to the COM of the payload (but can be approximated as the tip of the tether because the payload characteristic dimension is usually much smaller than the tether length). $r_{P1}, r_{P2}, r_{P3}, r_{P4}$ and r_{P5} are the radii of point P on orbits 1, 2, 3, 4 (trajectory) and 5 respectively. L_1 and L_2 are the sub-span of tethers 1 and 2 respectively. Orbit 1 is considered to be the base for calculations and the radii of point P on the other orbits are stated in terms of r_{P1} and the tether sub-span. The values of r_{P2}, r_{P3}, r_{P4} and r_{P5} are given by Equations (1) - (4).

$$r_{P2} = r_{P1} + L_1 \quad (1)$$

$$r_{P3} = r_{P1} + 2L_1 + L_2 \quad (2)$$

$$r_{P4} = r_{P1} + 2L_1 \quad (3)$$

$$r_{P5} = r_{P1} + 2L_1 + 2L_2 \quad (4)$$

The time period of parking orbit P_1 is taken as the base time period for the calculations and is given by Equation (5). The time period of orbits 2, 3, and 5 are denoted by P_2, P_3, and P_5 respectively and are related to each other as shown by Equations (6) - (8). l, m, and n are the orbital harmonics and a_1, a_2, a_3, and a_5 are the semi-major axes of orbits 1, 2, 3 and 5 respectively. This ensures that the second condition is met.

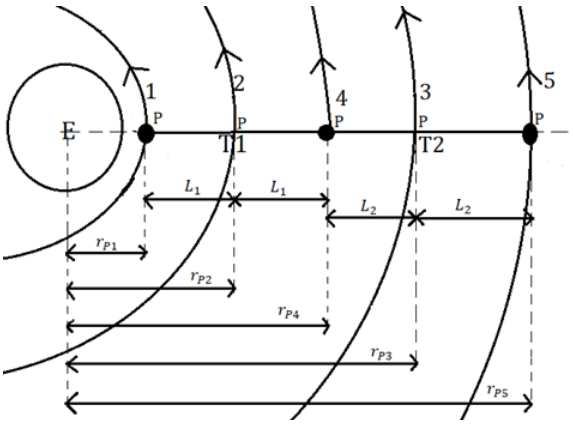

Figure 3: Important distances and tether sub-span considered in this study

$$P_1 = 2\pi\sqrt{\frac{a_1^3}{\mu_E}} \quad (5)$$

$$P_2 = l\,P_1 \Rightarrow a_2 = l^{\frac{2}{3}}a_1 \qquad l = 2,3,4,5\ldots \quad (6)$$

$$P_3 = m\,P_2 \Rightarrow a_3 = m^{\frac{2}{3}}a_2 \qquad m = 2,3,4,5\ldots \quad (7)$$

$$P_5 = \frac{1}{n}\,P_3 \Rightarrow a_5 = \frac{1}{n^{\frac{2}{3}}}a_3 \qquad n = 2,3,4,5\ldots \quad (8)$$

The velocities at point P of orbits 1, 2, 3 and 5, and trajectory 4 are denoted by V_{P1}, V_{P2}, V_{P3}, V_{P5}, and V_{P4} respectively and are given by Equations (9) and (10). $\mu_{E/M}$ denotes the gravitational parameter of Earth or Mars depending on which planet is under consideration.

$$V_{Pi} = \sqrt{\mu_{E/M}\left(\frac{2}{r_{Pi}} - \frac{1}{a_i}\right)} \qquad i = 1,2,3,5 \quad (9)$$

$$V_{P4} = \sqrt{V_\infty^2 + \frac{2\mu_{E/M}}{r_{P4}}} \quad (10)$$

V_∞ is the excess velocity that the payload must possess as it enters/exits the SOI of the planet. The excess velocity of the payload when it enters/exits the Earth's and Mars's SOI is given by Equations (11) and (12) respectively.

$$V_\infty = \sqrt{\frac{\mu_S}{r_E}}\left(\sqrt{\frac{2r_M}{r_E+r_M}} - 1\right) = 2.945km/s \quad (for\ Earth) \quad (11)$$

$$V_\infty = \sqrt{\frac{\mu_S}{r_M}}\left(1 - \sqrt{\frac{2r_E}{r_E+r_M}}\right) = 2.649km/s \quad (for\ Mars) \quad (12)$$

Assume that the tethers, payloads, and dummy payloads, orbit the planet in counter-clockwise direction as shown in Figure 3. ω_{t1} and ω_{t2} are the angular velocities of tether 1 and 2 respectively. Note that these angular velocities have a fixed value, not throughout the entire orbit, but only when tethers are at point P and in vertical orientation. It is the task of the control system to ensure these conditions are met and is not the scope of this study. ω_{t1} is positive for counter-clockwise rotation because tether 1 rotates prograde, while ω_{t2} is positive for clockwise rotation, due to tether 2's retrograde rotating. Condition one states that the relative velocity during handover/capture must be zero. Consider tether 1, T1 in orbit 2 and payload, p1 in orbit 1 during step 2 of outgoing phase. p1's velocity at point P in orbit 1 is V_{P1}. T1's velocity at point P in orbit 2 is V_{P2}, but the lower tip's velocity is $V_{P2} - \omega_{t1}L_1$ (prograde rotating). To achieve zero relative velocity condition during capture, T1's lower tip velocity (at P in orbit 2) must be equal to p1's velocity (at P in orbit 1), hence we obtain Equation (13). If we consider handover of dummy payload d1, from tether 2, T2 to T1 (in step 2 of outgoing phase) than the upper tip velocity of T1 which is $V_{P2} + \omega_{t1}L_1$, must be equal to the lower tip velocity of T2 which is $V_{P3} + \omega_{t2}L_2$ (retrograde rotating). However, the velocity at upper tip of T1 must equal to V_{P4}, to ensure that the payload has the required excess velocity as it exits the planet's SOI, thus obtaining Equation (*14*). This implies that the lower tip velocity of T2 must also be equal to V_{P4}, to ensure zero relative velocity condition during handover of d1 from T2 to T1, thus obtaining Equation (*15*). Equation (16) can be obtained by applying similar reasoning to T2 and dummy payload d2 in orbit 5.

$$V_{P1} = V_{P2} - \omega_{t1}L_1 \quad (lower\ tip\ tether\ 1) \quad (13)$$

$$V_{P4} = V_{P2} + \omega_{t1}L_1 \quad (upper\ tip\ tether\ 1) \quad (14)$$

$$V_{P4} = V_{P3} + \omega_{t2}L_2 \quad (lower\ tip\ tether\ 2) \quad (15)$$

$$V_{P5} = V_{P3} - \omega_{t2} L_2 \quad (upper\ tip\ tether\ 2) \qquad (16)$$

The above derived Equations (1) - (16), have 5 independent variables: l, m, n, r_{P1} and a_1. The primary aim is to determine the tether angular velocities and tether sub-span, after which the orbital parameters can be calculated. By choosing appropriate values of l, r_{P1} and a_1, values of ω_{t1} and L_1 can be calculated by solving Equations (13) and (14). After which the values of r_{P2}, r_{P4}, and a_2 can be calculated from Equations (1), (3) and (6). The values of ω_{t2} and L_2 can be calculated by solving Equations (15) and (16), by choosing some values of m and n. After which the values of r_{P3}, r_{P5}, a_3 and a_5 can be calculated from Equations (2), (4), (7) and (8).

5 DECAY OF ORBITS DUE TO DRAG PERTURBATION AND A METHODOLOGY TO DETERMINE THE DECAY

A round trip to Mars from Earth and to Earth from Mars takes 2.663 years and 1.945 years respectively. Once the payload leaves the planet, the dummy payloads, d1 and d2, and the tethers T1 and T2 will be in their respective orbits for a long time, i.e. until the payload returns from the other planet. Over time these four orbits will decay due to the effects of the atmospheric drag force. Thus, the dummy payloads and tethers will need to re-raise their orbits by means of some propulsion system. If conventional chemical propulsion or ion/plasma propulsion is used then the mass of the dummy payloads (as well as the tethers) will decrease. Therefore, the payload that is returning from Mars needs to possess less mass than it had before, in order to balance the tethers. As the transfers are carried out, the mass of the payload that can be sent to the other planet will decrease until these dummy payloads no longer have any propellant remaining to raise their orbit. New dummy payloads will be needed to replace the old ones so that the transfer process can continue.

Cowell's method [8] is a straightforward approach for simulating the orbit/trajectory of a minor body around another major body, using direct numerical integration of the 2-body equation of motion. Cowell's method has been used in this orbital decay study as the objective is to gain an approximate idea of orbital decay due to drag, without seeking high precision. The 2-body equations of motion (where the mass of major body is significantly greater than that of minor body) in general form are shown by Equations (17) and (18). 2D cartesian coordinate system is considered for this study. As seen from the top (Figure 3), the x axis passes through point P from centre of the planet, and y axis is vertical and upwards (i.e. along the upper semi-latus rectum). Atmospheric drag is modelled as a quadratic effect. The quadratic drag model is a relatively simple but reasonably effective model and has provided accurate results in many real-world applications. $V_i, \bar{u}, u, t, \rho, S, C_D$ and m_p are respectively, the velocity in the desired direction (V_x or V_y), the displacement vector ($x\hat{\imath} + y\hat{\jmath}$), the displacement in the required direction (x or y), the time, the atmospheric density, the frontal area, the coefficient of drag, and the mass of the dummy payload/tether motor facility. The nominal atmospheric density variation with altitude of both Earth and Mars is obtained from the US Standard Atmosphere 1976 [8] and from the MarsGRAM report released by NASA [10], respectively.

$$\frac{d\,V_u}{dt} = -\frac{\mu_{E/M}\,u}{|\bar{u}|^3} - \frac{\rho V_u\,|V_u|\,SC_D}{2m_p} \qquad u = x\ or\ y \qquad (17)$$

$$\frac{d\,u}{dt} = V_u \qquad u = x\ or\ y \qquad (18)$$

A 2D Cartesian coordinate system is used in this study, hence, i is x or y. Since the values of r_P and a of each orbit are known the initial values can be calculated from Equations (19) - (22). The shape, dimensions, mass, and coefficient of drag considered for the payload and motor facility are shown in Table 3. The coefficient of drag is taken from Moe *et al*. [11] and is assumed to be constant. The final values of x, y, V_x and V_y were obtained and the new orbital parameters were found using Algorithm 4.2, from Curtis [8]:

$$x(t=0) = r_{Pi} \qquad i = 1, 2, 3, 5 \qquad (19)$$

$$y(t=0) = 0 \qquad (20)$$

$$V_x(t=0) = 0 \qquad (21)$$

$$V_y(t=0) = \sqrt{\mu\left(\frac{2}{r_{Pi}} - \frac{1}{a_i}\right)} \qquad i = 1, 2, 3, 5 \qquad (22)$$

Table 3: Assumed shape, dimensions, mass and CD of payload and central motor facility

	Dummy payload	**Motor facility**
Shape	Sphere	Cylinder
Radius (m)	0.5	0.5
Height (m)	-	1
Coefficient of Drag, C_D	2.123	2.170 (curved surface facing the flow)
Mass, m_p (kg)	1000	5000

6 RESULTS AND DISCUSSION

6.1 Orbits around Earth and Mars

Table 4 and Table 5 shows some results obtained for certain combinations of of l, m, n, r_{P1} and a_1 for possible orbits around Earth and Mars, respectively.

Table 4: Possible orbits around Earth

Sr no.	l	m	n	r_{P1} (km)	a_1 (km)	L_1 (km)	L_2 (km)	ω_{t1} (rad/s)	ω_{t1} (rad/s)
1	3	3	4	10000	8300	88.906	187.75	0.02079	0.006472
2	3	3	4	11400	9000	97.504	498.509	0.01916	0.002682
3	4	3	5	7000	10000	540.58	182.084	0.001624	0.005121
4	4	3	5	7500	10000	638.822	110.933	0.001428	0.008245
5	4	4	6	7000	11000	328.523	180.499	0.002752	0.004552
6	4	4	6	7500	11000	404.549	117.842	0.002297	0.006787
7	5	2	6	7000	15000	352.773	150.976	0.001765	0.005327
8	5	2	6	7500	15000	414.774	96.043	0.001553	0.008209
9	5	3	8	7000	16600	70.889	47.603	0.01049	0.01317
10	5	3	8	7500	16600	113.99	13.023	0.006597	0.04786
11	5	4	9	7000	16000	185.252	114.352	0.003715	0.005717
12	5	4	9	7500	16000	233.921	72.181	0.003005	0.008877
13	5	5	10	7000	15700	237.434	213.289	0.002804	0.003295
14	5	5	10	7500	15700	289.766	142.418	0.002357	0.004674
15	5	6	12	7000	16800	27.672	169.468	0.02774	0.003797
16	5	6	12	7500	16800	69.995	112.472	0.01103	0.005444
17	6	2	8	7000	19500	149.308	119.365	0.00399	0.005707
18	6	2	8	7500	19500	189.56	76.593	0.003206	0.008715
19	6	3	10	7000	19500	149.308	204.986	0.00399	0.003396

Point Q (which is not shown in Figure 2) lies opposite to point P. Although not calculated and shown here, point Q is the apoapsis of orbits 2 and 3 around Earth and Mars for all the cases considered. Point Q is the periapsis of orbits 1 and 4 around Mars and the periapsis of orbit 1 for the first result of the orbit around Earth. Orbits 2 and 3 are highly eccentric orbits, with most of them having radii of the point Q above 50,000 km. This allows both the tethers' tips at point P of trajectory 4 to have very high velocity – close to the escape velocity of the planet, but below it. The additional velocity required to launch or capture the payload from HET and HRT is provided by the rotating tether.

Result 3 from Table 4 was chosen arbitrarily to observe the trend of the four dependent variables (tether sub-spans L_1 and L_2, and tether in-plane angular velocities ω_{t1} and ω_{t2}), in relation to the independent variables. The value of each independent variable was varied while the others remained constant. Figure 4 shows the variations of L_1 and ω_{t1} with r_{P1}, a_1, and l. The orbital harmonics m and n do not affect the values of L_1 and ω_{t1}. The plots show only the real and positive portion of the trend (which is relevant to this study). Clearly, there is an opposite trend between L_1 and ω_{t1}, which is expected because the tether tip velocity is the product of these two variables. L_1 increases as r_{P1} and l increase. L_1 appears to reach infinity as r_{P1} approaches the major axis (twice the value of a_1) and negative infinity

as l becomes less than 4. Furthermore, L_1 decreases with an increase in a_1. Values of L_1 appear to be bounded between a_1 = 3800 km and a_1 = 12000 km, beyond which it becomes infinity or negative.

Table 5: Possible orbits around Mars

Sr no.	l	m	n	r_{P1} (km)	a_1 (km)	L_1 (km)	L_2 (km)	ω_{t1} (rad/s)	ω_{t1} (rad/s)
1	17	2	29	9900	7000	95.996	226.391	0.01222	0.005121
2	17	2	29	10100	7000	247.017	77.33	0.004755	0.01497
3	17	3	41	9900	7000	95.996	314.434	0.01222	0.003649
4	17	3	41	10100	7000	247.017	166.447	0.004755	0.006878
5	17	3	42	9900	7000	95.996	166.545	0.01222	0.006761
6	18	2	31	9700	7000	80.245	194.965	0.01443	0.005857
7	18	2	31	9900	7000	224.164	53.267	0.005173	0.02141
8	18	3	44	9700	7000	80.245	263.449	0.01443	0.004284
9	18	3	44	9900	7000	224.164	123.074	0.005173	0.009154
10	18	3	45	9700	7000	80.245	129.648	0.01443	0.008552
11	19	2	32	9600	7000	125.467	293.867	0.009123	0.003923
12	19	2	32	9800	7000	265.877	152.465	0.004313	0.007546
13	19	3	46	9600	7000	125.467	293.713	0.009123	0.003848
14	19	3	46	9800	7000	265.877	155.032	0.004313	0.007274
15	19	3	47	9600	7000	125.467	164.044	0.009123	0.006772
16	20	2	34	9400	7000	94.400	276.897	0.01199	0.004108
17	20	2	34	9700	7000	297.774	73.062	0.003811	0.01553
18	20	3	49	9400	7000	94.400	266.792	0.01199	0.004176
19	20	3	49	9700	7000	297.774	67.11	0.003811	0.01656

Figure 5 show the variations of L_2 and ω_{t2} with r_{P1}, a_1, and l. The orbital harmonics m and n do affect the values of L_2 and ω_{t2} but, in this case, solutions only exist for $m = 3$ and $n = 5$. The plots show only the real and positive portion of the trend. There is an opposite trend between L_2 and ω_{t2}. Secondly, the ranges of r_{P1}, a_1, and l have decreased within which positive real solutions exists. l in this case has solutions of L_2 at only 4, 5, and 6 whereas in the previous case, there appeared to be a solution for L_1 at any integer value of l greater than 3. L_2 increases as l increases, which is similar to the previous trend of L_1 and l. L_2 decreases as r_{P1} increases and increases when a_1 increases. This is opposite to the trend of L_1 in relation to r_{P1} and a_1.

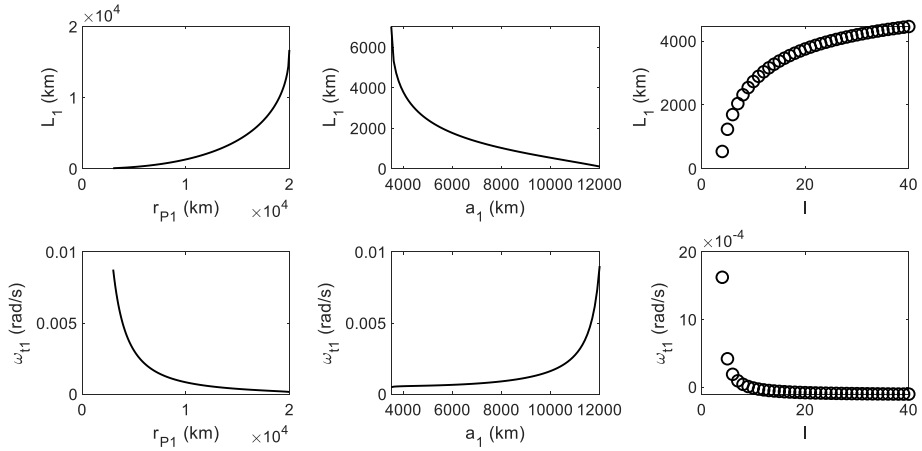

Figure 4: Variation of L_1 and ω_{t1} with r_{p1}, a_1 and l

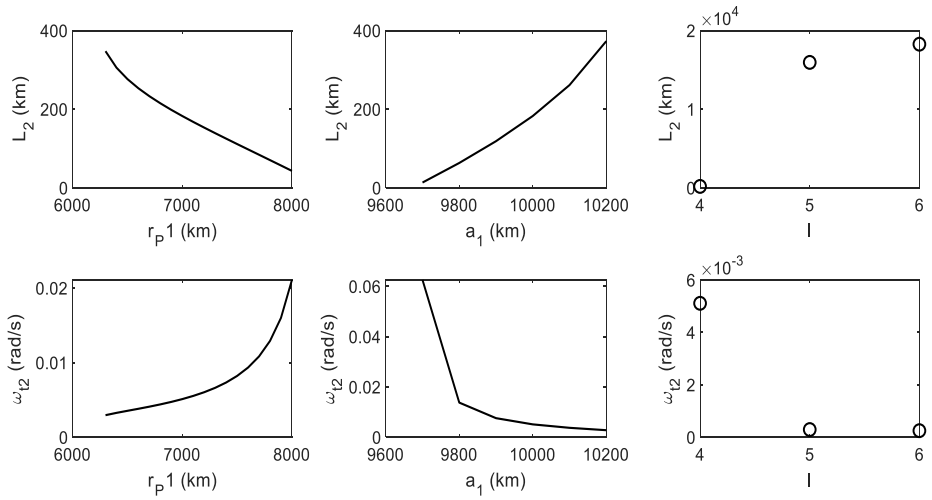

Figure 5: Variation of L1 and ω_{t2} with rp1, a1 and l

A suitable solution is one that has a tether sub-span of less than 300 km. Short tethers are easier to control, but a shorter tether may require its orbit to be highly eccentric to gain extra velocity at point P and/or to have a higher angular velocity. Hence, result 9 from Table 4 and result 10 from Table 5 might be suitable solutions for orbits around Earth and Mars, respectively.

6.2 Orbit Decay

Table 6: r_P and a of orbits around Earth before and after 2.336 years

Before		After		Percentage Change	
r_P (km)	a (km)	r_P (km)	a (km)	$\frac{\Delta r_P}{r_P}$ %	$\frac{\Delta a}{a}$ %
Orbit 1					
7000	16600	6983.985	16589.038	-0.229	-0.066
Orbit 2					
7070.889	48528.694	7036.060	48524.551	-0.493	-0.00853
Orbit 3					
7189.381	100964.553	7169.117	100973.484	-0.282	0.00885
Orbit 5					
7236.984	25241.138	7215.755	25229.914	-0.293	-0.0445

Table 7: r_P and a of orbits around Mars before and after 1.945 years

Before		After		Percentage Change	
r_P (km)	a (km)	r_P (km)	a (km)	$\frac{\Delta r_P}{r_P}$ %	$\frac{\Delta a}{a}$ %
Orbit 1					
9700	7000	9694.341	6999.524	-0.0583	-0.0068
Orbit 2					
9780.245	48077.998	9759.468	48076.195	-0.212	-0.00375
Orbit 3					
9990.138	100006.266	10000.949	100009.493	0.108	0.00323
Orbit 5					
10119.786	7904.703	10111.027	7905.416	-0.0866	0.00902

The orbits around Earth (result 9 from Table 4) were simulated for 2.663 years i.e. the time of a round trip to Mars, and the orbits around Mars (result 10 from Table 5) were simulated for 1.945 years i.e. the time of a round trip to Earth. The comparison of the initial and final values of r_P and a for each orbit, and the percentage change $\frac{\Delta r_P}{r_P}$ % and $\frac{\Delta a}{a}$ %, are shown in Table 6 and Table 7, respectively. The drag perturbation acts opposite to the direction of motion. This perturbation tries to slow down the orbiting dummy payloads and tether facilities and slowly lowers the radii of periapsis and apoapsis of their corresponding orbits. Since in this case only the drag perturbation is considered, a negative percentage change of r_P and a is expected.

As can be seen from Table 6 and Table 7 the percentage changes of r_P and a are negative and below 1% for most orbits, which indicates that the decay of the orbits is negligible. The r_P and/or a of Orbit 3 from Table 6 and Orbits 3 and 5 from Table 7 have positive percentage changes. This might be due to negligible drag force and some numerical error accumulated over time. This small perturbation of the orbit due to drag can be corrected easily by minimal use of propellants or by other non-conventional propulsion means.

7 FAILURE SCENARIOS AND RECOVERY SYSTEM

This section discusses some major scenarios that can occur in cases where the tether fails to capture the payload or the dummy payload, as well as the possible recovery strategy that will get the system back to its normal operation. A reasonable operational assumption is made that the release of the payload by the tether during handover is always successfully achieved.

7.1 Outgoing phase

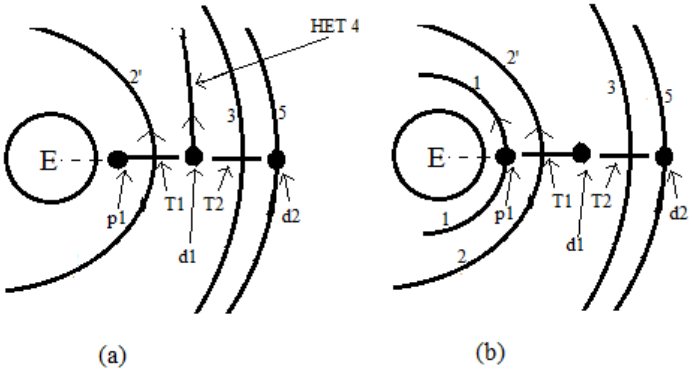

Figure 6: Outgoing phase failure scenarios (a) Failure scenario 1, (b) Failure scenario 2

During the outgoing phase, two major failure scenarios can occur. Consider that payload p1 is in parking orbit 1. Failure scenario 1 (Figure 6 (a)) occurs when T1 captures p1 from orbit 1 but fails to capture d1 from T2. If this happens, then T1 will be asymmetrically laden and the COM will shift towards p1. This will cause T1 to go into a lower orbit 2'. If T1 immediately releases p1, then there would not be much perturbation in T1's and p1's orbits and these can be readjusted using the onboard propulsion system. Since T1 has failed to capture d1, d1 will be released into trajectory 4 (HET). Below are the recovery options:

a. In this case, a spaceplane such as an hypersonic airplane HASTOL [12], will be needed to capture d1 before it escapes the planet's SOI. The spaceplane may already be stationed on a facility orbiting the planet. Once captured, d1 may be released in an orbit to rendezvous with T1 at point P or
b. The dummy payload can be abandoned and a new dummy payload will be needed to replace it. The new dummy payload may be launched from the planet or from a dummy payload storage facility already orbiting the planet.

If the dummy payload is abandoned, it will arrive on the other planet where it can be captured by the dummy payload storage facility and prepared for the next failure event.

Failure scenario 2 (Figure 6 (b)) occurs when T1 captures d1 from T2 but fails to capture p1 from orbit 1. p1 will remain in orbit 1 and the capture can be attempted later. But the COM of T1 will shift upwards towards d1. This will cause T1 to go into a higher orbit 2'. Below are the recovery options:

a. T1 immediately lets go of d1 after the failed capture of p1. The orbit of T1 will be slightly perturbed but can be readjusted using the onboard propulsion system. But d1 will most probably have sufficient velocity to escape the planet, but may not have enough excess velocity to reach the other planet. This

dummy payload will orbit the Sun if left undisturbed, therefore it will need to be recovered using a spaceplane. If recovered, then that dummy payload can be reused or a new one can be deployed through the dummy payload storage facility orbiting the planet or

b. Tether T1 can release d1 after a certain time and at a different tether angular displacement such that d1 does not escape the planet's SOI. This dummy payload d1 can be recovered by the spaceplane at a later time. But by the time T1 releases d1, T1's orbit will have been considerably perturbed and comparably more delta-v will be required to get T1 to its original orbit.

7.2 Return Phase

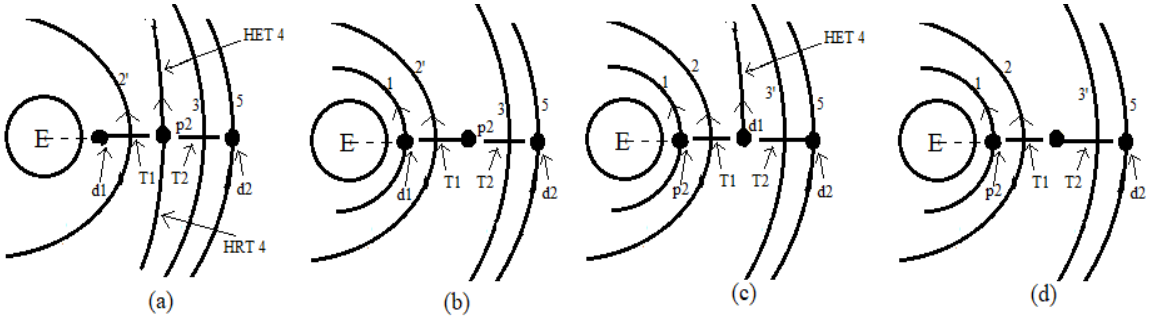

Figure 7: Return phase failure scenarios (a) Failure scenario 3, (b) Failure scenario 4, (c) Failure scenario 5, (d) Failure scenario 6

During the return phase, four major failure scenarios can occur. Consider that payload p2 is in HRT 4. Failure mode 3 (Figure 7 (a)) occurs when T1 captures d1 from orbit 1 but fails to capture p2 from HRT. This scenario is similar to Failure mode 1. T1 will be asymmetrically laden and the COM will shift towards d1. This will cause T1 to go into a lower orbit 2'. If T1 immediately releases d1, then there would not be much perturbation in T1's and d1's orbits and it can be readjusted using the onboard propulsion system. Since T1 has failed to capture p2, p2 will continue in trajectory 4 (HET). A spaceplane will be needed to capture it and return it to the planet. However, neither of the dummy payloads are at T2 which is the configuration that would be required to launch a payload in HET 4 to escape the planet's SOI. In this case,

a. The spaceplane can release the captured payload p2 along HRT 4 so it can rendezvous with T1 at P and normal tether operation can continue or
b. Another spaceplane can carry d1 to a higher orbit so that T2 can capture d1 and d2 or
c. Another dummy payload can be deployed by the dummy payload storage facility to rendezvous with T2, and the old dummy payload d1 can be captured and prepared for another failure event.

Failure mode 4 (Figure 7 (b)) occurs when T1 captures p2 from HRT 4 but fails to capture d1 from orbit 1. This scenario is similar to Failure mode 2. T1 will become asymmetrically laden and the COM will shift upwards towards p2. This will cause T1 to go into a higher orbit 2'. In this case, T1 cannot let go of p2 immediately or else it will most probably have enough velocity to escape the planet's SOI. Instead, the second recovery option of Failure mode 2 needs to be followed. The payload p2 can later be deorbited by the spaceplane and T1 can readjust its orbit using the onboard propulsion system. But both the dummy payloads are not at T2, which is the configuration that would be required to launch a payload in HET 4 to escape the planet's SOI, noting the similarity to Failure mode 3. Recovery options b and c can be followed to resume normal tether operation.

Failure mode 5 (Figure 7 (c)) occurs when T2 captures d2 from orbit 5 but fails to capture d1 from T1. The COM of T2 shifts upwards towards d2. This will cause T2 to go into a higher orbit 3'. If T2 immediately releases d2 then there will not be much perturbation in T2's and p2's orbit and this can be readjusted using the onboard propulsion system. Since T2 has failed to capture d1, d1 will be released into trajectory 4 (HET). A spaceplane will be needed to capture it. The spaceplane may hand d1 to T2, or a new dummy payload may be released by the dummy payload storage facility to replace d1. d1 can be returned to the dummy payload storage facility and prepared for future failure events.

The final failure mode, i.e. Failure mode 6 (Figure 7 (d)) occurs when T2 captures d1 from T1 but fails to capture d2 from orbit 5. If this is the case then, d2 will remain in its original orbit and the capture can be attempted later. T2 will be asymmetrically laden and the COM will shift downwards towards d1. This will cause T2 to go into a lower orbit 3'. This is similar to Failure mode 2, except with T2. Similar recovery options, as mentioned in Failure mode 2, can be used to capture d1 and resume normal tether operations.

8 CONCLUSIONS

A methodology has been developed based on a proposed symmetrical MMET logistical system for the continuous two-way transfer of payloads between Earth and Mars, to identify the possible orbits of tethers and their dummy payloads around both Earth and Mars, taking into consideration the necessity of reusable dummy payloads. Symmetrical tethers have the advantage of maintaining their orbit during the simultaneous capture or release of equal payloads at both their ends, thus eliminating the need to readjust their orbit. Some physically possible orbits are presented, and a sensitivity analysis has been performed. An atmospheric drag perturbation study has also been conducted to determine the decay of the orbits of the tethers and the dummy payloads during the interval between the departure of the payload from one planet until the return of the payload from the other planet. The analyses showed that the decay of the orbits is generally negligible due only to atmospheric drag perturbations.

The proposed methodology can be extended to transfers between other planets by changing the required excess velocity. This study just presents a small portion of the possible orbits around Earth and Mars based on the developed methodology. A simple observation is that shorter tethers are easier to control and therefore could be operationally preferable, but it's also the case that shorter tethers will require a higher motor angular velocity to achieve the required tip speed. So in such cases, it may well take a considerable amount of time to spin up or spin down the tether, confirming that there must be a trade-off between the tether sub-span length and the angular velocity. This problem can be thought of as an optimisation problem with the tether sub-span and angular velocity as the objective functions, and the orbital harmonics, minimum and maximum orbit altitude, and the allowed range of the tether sub-span and the system's angular velocity all as the constraints.

In reality, planetary orbits deviate from the circular and coplanar configurations assumed for this preliminary study, introducing complexities such as orbital inclination and the potential limitations of Hohmann transfers. This methodology could therefore be extended to the 3D domain, and to consider different transfer windows with different excess velocity requirements. Main failure scenarios and recovery strategies are discussed here, but further studies, especially on the spaceplane and the dummy payload storage facility will be necessary to evaluate these strategies.

ACKNOWLEDGEMENTS

The authors would like to thank the technical staff and management team of the University of Strathclyde for their valuable assistance in acquiring the necessary software licenses and granting access to resources crucial for the completion of this research.

REFERENCES

1. Puig-Suari, J., Longuski, J., and Tragesser, S. "A tether sling for lunar and interplanetary exploration," Acta Astronautica Vol. 36, No. 6, 1995, pp. 291-295.
2. Forward, R., and Nordley, G. "Mars-Earth Rapid Interplanetary Tether Transport (MERITT) system. I-Initial feasibility analysis," 35th Joint Propulsion Conference and Exhibit. 1999, p. 2151.
3. Cartmell, M., and Ziegler, S. "Symmetrically laden motorised tethers for continuous two-way interplanetary payload exchange," 35th Joint Propulsion Conference and Exhibit. 1999, p. 2840.
4. Hoyt, R. P., and Uphoff, C. "Cislunar tether transport system," Journal of Spacecraft and Rockets Vol. 37, No. 2, 2000, pp. 177-186.
5. Accettura, A. G., Bruno, C., Casotto, S., and Marzari, F. "Mission to Mars using integrated propulsion concepts: considerations, opportunities, and strategies," Acta Astronautica Vol. 54, No. 7, 2004, pp. 471-486.
6. Jokic, M. D., and Longuski, J. M. "Design of Tether Sling for Human Transportation System Between Earth and Mars," Journal of spacecraft and rockets Vol. 41, No. 6, 2004, pp. 1010-1015.
7. Knapman, J. M., and Swan, P. A. "Secondary tethers," Acta Astronautica Vol. 195, 2022, pp. 561-566.
8. Curtis, H. D. Orbital mechanics for engineering students: Butterworth-Heinemann, 2013.
9. Hoyt, R. "Design and simulation of a tether boost facility for LEO to GTO transport," 36th AIAA/ASME/SAE/ASEE Joint Propulsion Conference and Exhibit. 2000, p. 3866.
10. Alexander, M. "Mars Transportation Environment Definition Document." National Aeronautics and Space Exploration, 2001.
11. Moe, K., Moe, M. M., and Wallace, S. D. "Improved satellite drag coefficient calculations from orbital measurements of energy accommodation," Journal of spacecraft and rockets Vol. 35, No. 3, 1998, pp. 266-272.

12. Grant, J., Willenberg, H., Tillotson, B., Stemler, J., Bangham, M., and Forward, R. "Hypersonic airplane space tether orbital launch: HASTOL-A two-stage commercial launch system," 36th AIAA/ASME/SAE/ASEE Joint Propulsion Conference and Exhibit. 2000, p. 3841.